

The Perivascular Astroglial Sheath Provides a Complete Covering of the Brain Microvessels: An Electron Microscopic 3D Reconstruction

THOMAS MISJE MATHISEN, KNUT PETTER LEHRE, NIELS CHRISTIAN DANBOLT,
AND OLE PETTER OTTERSEN*

Centre for Molecular Biology and Neuroscience, Department of Anatomy, Institute of Basic Medical Sciences,
University of Oslo, N-0317 Oslo, Norway

KEY WORDS

three-dimensional reconstruction; blood–brain barrier; AQP4; blood flow; pericyte

ABSTRACT

The unravelling of the polarized distribution of AQP4 in perivascular astrocytic endfeet has revitalized the interest in the role of astrocytes in controlling water and ion exchange at the brain–blood interface. The importance of the endfeet is based on the premise that they constitute a complete coverage of the vessel wall. Despite a number of studies based on different microscopic techniques this question has yet to be resolved. We have made an electron microscopic 3D reconstruction of perivascular endfeet in CA1 (stratum moleculare) of rat hippocampus. The endfeet interdigitate and overlap, leaving no slits between them. Only in a few sites do processes—tentatively classified as processes of microglia—extend through the perivascular glial sheath to establish direct contact with the endothelial basal lamina. In contrast to the endfoot covering of the endothelial tube, the endfoot covering of the pericyte is incomplete, allowing neuropil elements to touch the basal lamina that enwraps this type of cell. The 3D reconstruction also revealed large bundles of mitochondria in the endfoot processes that came in close apposition to the perivascular endfoot membrane. Our data support the idea that in pathophysiological conditions, the perivascular astrocytic covering may control the exchange of water and solutes between blood and brain and that free diffusion is limited to narrow clefts between overlapping endfeet. © 2010 Wiley-Liss, Inc.

INTRODUCTION

One hundred and fifty years have passed since Virchow first described a relationship between glial cells and vessels in brain (Virchow, 1858) and 140 years since Golgi showed that glial branches were directly attached to vessels (Golgi, 1871). Surprisingly, there is as yet no consensus as to the 3D structure of these glial processes, commonly called perivascular endfeet.

Glees (1955) defined the perivascular endfoot as “the little end plate of an astrocyte process terminating on a cerebral vessel wall,” while he referred to the envelopment of the vascular wall by astrocytic end feet as the glial barrier, and the multitude of end plates as “membrana limitans gliae perivascularis.” The advent of the

electron microscope paved the way for a number of descriptive studies of the glial sheath, based on analysis of ultrathin sections (Bär and Wolff, 1977; Farquhar and Hartman, 1957; Maynard et al., 1957; Mugnaini and Walberg, 1965a; Wolff, 1963) or freeze fracture preparations (Gotow and Hashimoto, 1984; Landis and Reese, 1974; Neuhaus, 1990; Rash et al., 2004; Wolburg, 1995). Since the mid 1990s the use of immunolabeling techniques has revealed a multitude of different membrane proteins in endfeet membranes (Lehre et al., 1995; Nielsen et al., 1997). Recently, the morphology of endfeet has been studied quite extensively by confocal microscopy (El-Khoury et al., 2006; Kacem et al., 1998; Oberheim et al., 2009; Simard et al., 2003) and a couple of studies have provided reconstructions of endfeet based on serial thin sections (Bertossi et al., 1989, 1993; Roncali et al., 1989). The latter studies were done in chick embryos.

The present study aims to provide a detailed 3D reconstruction of astrocytic endfeet in rat brain. Specifically, we set out to establish whether the endfeet provide a complete covering of the brain microvessels. If so, the endfeet may serve as a relative barrier in pathophysiological conditions that are characterized by a large flux of water or solutes across the brain–blood interface. A relative barrier imposed by the endfoot coverage would come in addition to the barrier that is served by the endothelial cells, commonly considered the morphological substrate for the barrier function at the blood–brain interface (Ballabh et al., 2004).

Endfeet are not coupled by tight junctions and the clefts between them—regardless of width and length—will not be expected to restrict movement of water and solutes under physiological conditions. The situation may be quite different in the build-up phase of brain edema when large amounts of water enter the brain in a

Grant sponsor: Research Council of Norway (STORFORSK and FRIBIOFYS) Private Funds.

*Correspondence to: Ole Petter Ottersen, Centre for Molecular Biology and Neuroscience, Department of Anatomy, Institute of Basic Medical Sciences, University of Oslo, P. O. Box 1105 Blindern, N-0317 Oslo, Norway.
E-mail: o.p.ottersen@medisin.uio.no

Received 1 October 2009; Accepted 23 February 2010

DOI 10.1002/glia.20990

Published online 29 March 2010 in Wiley InterScience (www.interscience.wiley.com).

relatively short time period. The perivascular glial sheath may then become rate limiting for water flux, but only if the endfeet overlap or abut on each other without intervening discontinuities. Indeed, the finding that edema formation is curbed by deleting AQP4 water channels from the perivascular glial sheath does suggest that endfeet restrict water passage when water flux is high (Amiry-Moghaddam and Ottersen, 2003).

In addition to generating data on the continuity of the perivascular glial sheath we also set out to provide essential information of relevance for neurovascular signaling. Most notably, as recent studies have identified pericytes as critical players in the regulation of microvascular blood flow we used our 3D reconstructions to resolve whether the pericytes are covered by endfeet or whether they are also exposed to other tissue elements that might be involved in regulating their contractile function. Finally, we asked whether the capillary basal lamina is in direct contact with tissue elements other than endfeet and pericytes. Any structure in direct contact with the capillary endothelial membrane could conceivably be involved in the maintenance of capillary structure or function.

MATERIALS AND METHODS

Tissue Preparation

Four male Wistar rats (7 weeks, about 300 g; from BK Scanbur, Nittedal, Norway), were used for the present analysis. The animals were anesthetized with 100 mg kg⁻¹ pentobarbital (50 mg mL⁻¹), and absence of corneal reflex was confirmed before transcatheter perfusion fixation (as described in Casella et al., 1997; Danbolt et al., 1998) followed by immediate dissection (Casella et al., 1997). The fixative was a mixture of 1% formaldehyde and 2.5% glutaraldehyde in 0.1 M sodium phosphate buffer pH 7.4 (NaPi) at 25°C. 500 mL fixative was delivered at 50 mL min⁻¹ following a rinse with 15 mL of Dextran 70 (Amersham Biosciences AB, Uppsala, Sweden) in NaPi. All procedures conform to National Institutes of Health guidelines for the care and use of laboratory animals.

The brains were stored in diluted fixative overnight before right hippocampus was dissected 3–4 mm from the temporal pole. Small tissue pieces including stratum lacunosum moleculare (CA1) were rinsed in NaPi before immersion in OsO₄ (10 mg mL⁻¹ in NaPi). After osmication, the tissue pieces were washed in NaPi and dehydrated in graded ethanols. To remove the last traces of water, we incubated specimens in propylene oxide. After immersion in Durcupan ACM[®] (Fluka, Sigma-Aldrich Chemie GmbH, Steinheim, Switzerland) for 30 min at 56°C, pieces were transferred to new Durcupan and left overnight at room temperature. Tissue pieces were finally put in capsules with Durcupan to polymerize at 56°C for 48 h.

Ultrathin sections of 45 nm were cut in series in an ultramicrotome from Leica (Vienna, Austria), before being contrasted with 10 mg mL⁻¹ uranyl acetate

(1 min) and 3 mg mL⁻¹ lead citrate (2 min). Sections were photographed with a Tecnai G2 electron microscope from FEI (Hillsboro, OR).

Morphometry and Statistical Analysis

In each of three animals, three series of consecutive ultrathin sections were obtained. Each series consisted of 10 sections and the individual series were separated by a distance of 50 μm. A total of 15–20 crosssectioned vessels were photographed from each of these nine series, giving a total of 164 vessels. All pictures were taken in stratum moleculare close to the hippocampal fissure, the most densely vascularized stratum of Cornu Ammonis (Duvernoy, 2005). Morphometrical measurements and 3D reconstruction were done using the software program RECONSTRUCT (Fiala, 2005). Statistical analyses were done using the Science Linker[®] database system (Science Linker AS, Oslo, Norway).

Serial Section Electron Microscopy and 3D Reconstruction

The fourth animal contributed with tissue for the 3D reconstruction, and the capillary chosen for reconstruction were located close to the middle of stratum moleculare CA1 (vide supra). We used the automated multiple imaging alignment (MIA) technology of the electron microscope to produce 5 × 5 montages from simple images with primary magnification 26,500×. Out of a total of 235 serially cut sections (Harris et al., 2006), seven pictures had to be excluded, and 228 sections were finally aligned and structures reconstructed in three dimensions using RECONSTRUCT.

RESULTS

What Structures Ensheath the Cerebral Capillaries?

Three different structural components were found to abut on the endothelial basal lamina

About one third (37%) of the circumference of the endothelial tube (here defined as the endothelial layer plus the underlying basal lamina) was covered by pericytes and their processes (Fig. 1, Table 1). The serrated nature of the pericytes was evident from the reconstruction. The analysis also revealed the presence of elongated mitochondria that ran parallel to the long axis of the pericyte cell body (see Fig. 1).

The criteria used to distinguish pericytes from other cell types (perivascular macrophages, dendritic cells, and microglial cells) were according to those published by Mercier et al. (2006) and Peters et al. (1991). Both pericytes and macrophages are encircled by a continuous basal lamina, but perivascular macrophages are less electron dense than pericytes. Unlike pericytes, perivascular

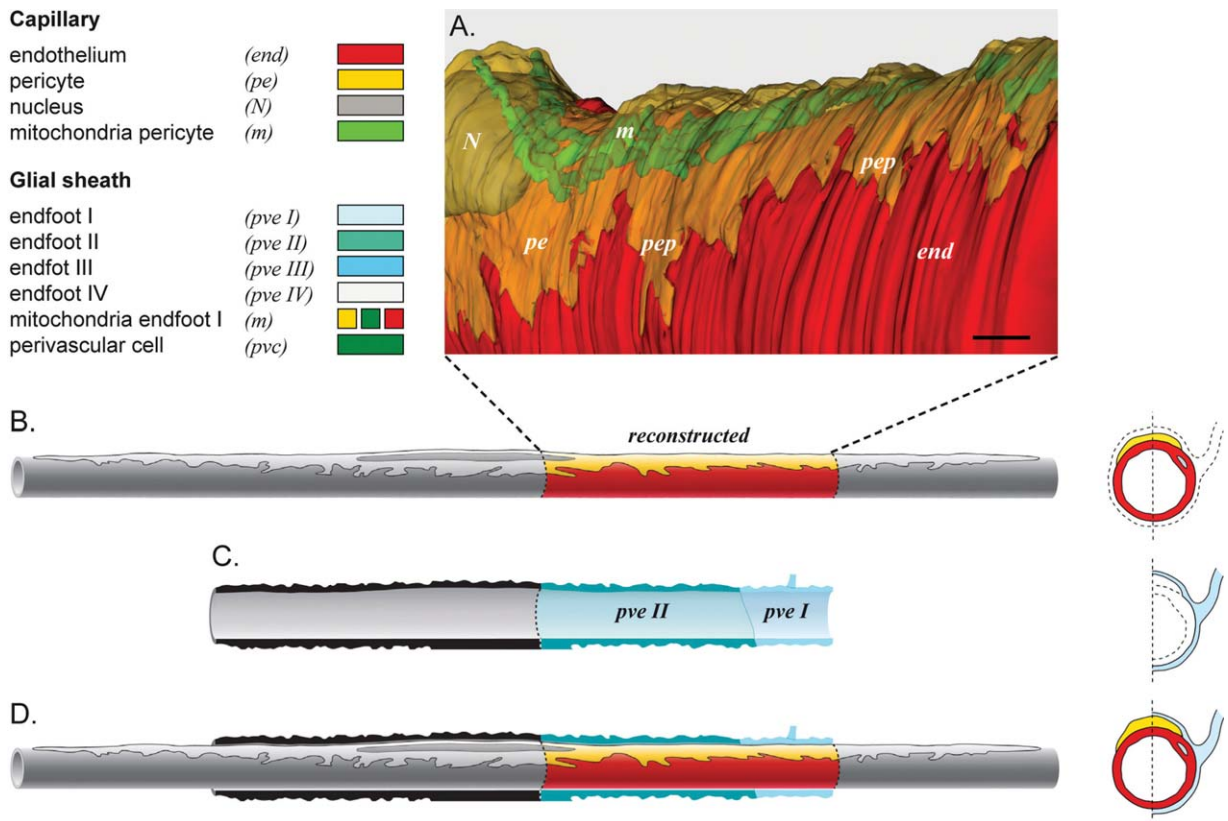


Fig. 1. Serrated nature of pericyte. The color scheme explains both 3D reconstructions and illustrations in this article, and is as far as practically possible based on guidelines for maintaining a consistent color scheme developed by Kristen M. Harris, available at Synapse Web, <http://synapses.clm.utexas.edu/>. (A) A pericyte (*pe*) resting on an endothelial tube (*end*) was reconstructed by serial section electron microscopy of rat hippocampus tissue from stratum moleculare in CA1. The pericyte border is typically serrated with long pericytic processes

(*pep*) embracing the vessel. Elongated mitochondria (*m*) follow the central core of the pericyte longitudinally from the cell nucleus (*N*) in distal direction. (B) A longer segment of the same cerebral capillary, with a colored area corresponding to the reconstruction, and with grey extrapolations to gain overview. The colored area is complementary to colored areas in (C), showing two perivascular endfeet *pve I* and *pve II*. (D) shows (B) and (C) merged. All structures are also shown in cross-sections. Scale bar = 1 μ m.

macrophages display nuclei with characteristic heterochromatin and a cytoplasm densely packed with organelles and lysosomes. Finally, pericytes typically have long, slender primary processes which branch extensively to form secondary processes (Díaz-Flores et al., 1991).

About two thirds (63%) of the endothelial tube are ensheathed by astrocytic endfeet (Table 1). Four endfeet, indexed pve I-IV, are represented in the reconstruction shown in Figs. 2–4. This reconstruction encompasses 10 μ m of vessel length and is based on a series of 235 consecutive sections. The reconstruction shows that the endfeet interdigitate without leaving any slits between them. Only in a few sites did we identify discontinuities in the astrocytic endfoot covering (Figs. 2–4). These discontinuities were small and could only be revealed after 3D reconstructions. Thus, the “holes” were missed in the single section analysis that formed the basis for the quantitative data in Table 1.

The discontinuities in the astrocytic covering of the endothelial tube were filled by processes (pvcp, Figs. 2–5) that were characterized by high electron density. Based on their ultrastructural features (short, stout protrusions without any lamellae and filopodia) these processes were

tentatively classified as processes of microglial cells (Peters et al., 1991).

In conclusion, the endothelial basal lamina is covered by two major components (pericytes and astrocytic endfeet) plus a minor component (possibly microglial processes) that connect to the basal lamina through the minute openings in the astrocytic covering.

Abluminal surface of pericytes

The 3D reconstruction shows astrocytic endfeet covering most of the abluminal surface of the pericytes, except for some irregularly shaped discontinuities (see Fig. 2). For practical reasons a full 3D reconstruction can be made only of select vessels. Thus, the statistical analysis was based on single sections comprising a large number of vessels (see methods). The statistical analysis (Table 1) indicates that less than 1% of the pericyte surface lacks endfoot covering. However, the single section analysis is likely to represent an underestimate because small discontinuities can be identified effectively only after 3D reconstruction.

TABLE 1. Glial Coverage of Capillaries from Hippocampal Stratum Moleculare CA1

Structure	Animal 1	Animal 2	Animal 3	Mean	SEM
Endothelium					
Endothelium with pericyte + endothelium without pericyte (μm)	14.0	13.2	12.9	13.3	0.33
Endothelium with pericyte/(endothelium with pericyte + endothelium without pericyte)	0.39	0.37	0.36	0.37	0.0066
Endothelium without pericyte/(endothelium with pericyte + endothelium without pericyte)	0.61	0.63	0.64	0.63	0.0066
Glial coverage of endothelium					
Endothelium with glia + endothelium without glia + endothelium undetermined glia (μm)	8.6	8.4	8.4	8.5	0.058
Endothelium with glia/(endothelium with glia + endothelium without glia + endothelium undetermined glia)	1	1	1	1	0
Endothelium without glia/(endothelium with glia + endothelium without glia + endothelium undetermined glia)	0	0	0	0	0
Endothelium undetermined glia/(endothelium with glia + endothelium without glia + endothelium undetermined glia)	0	0	0	0	0
Glial coverage of pericyte					
Pericyte with glia + pericyte without glia + pericyte undetermined glia (μm)	6.4	5.5	5.1	5.7	0.39
Pericyte with glia/(pericyte with glia + pericyte without glia + pericyte undetermined glia)	0.99	0.99	0.98	0.99	0.0043
Pericyte without glia/(pericyte with glia + pericyte without glia + pericyte undetermined glia)	0	0.0025	0.011	0.0046	0.0034
Pericyte undetermined glia/(pericyte with glia + pericyte without glia + pericyte undetermined glia)	0.0083	0.0032	0.0082	0.0066	0.0017
Intercellular clefts					
Mean number of clefts per vessel profile (= mean number of endfeet per image)	2.9	2.3	2.3	2.5	0.19
Mean number of cleft projections per vessel profile	2.9	2.3	2.3	2.5	0.19
Mean cleft value (μm)	0.50	0.36	0.49	0.45	0.044
Mean cleft projection value (μm)	0.36	0.27	0.34	0.32	0.30

Crosssections from a total of 164 capillaries from three animals were subjected to morphometrical analyses. First, we measured the circumference of the endothelial tube (here defined as the endothelial layer plus the underlying basal lamina) covered by pericytes. Second, we measured the percentage of the endothelial tube and pericyte ensheathed by astrocytic endfeet. Finally, the profile lengths of the intercellular clefts that separate contiguous endfoot processes were measured, as were the lengths of these clefts as projected on the endothelial basal lamina.

How do the Astrocytic Endfeet Relate to Each Other?

As noted above, the endfoot covering of the endothelial tube is almost complete. An important question is whether there is a significant overlap between adjacent endfoot processes or whether adjacent processes simply touch (separated only by the ~ 20 nm standard width of the extracellular space). On average, 2.5 transected intercellular clefts were identified per vessel profile. The lengths of the intercellular clefts (IC) that separate contiguous endfoot processes were measured, as were the projection lengths (P) of these clefts on the endothelial basal lamina (Fig. 5e, Table 1). The extent of overlap (EO) was expressed as the ratio between these two values (P/IC). If the intercellular cleft is perpendicular to the basal lamina the EO value will be zero. If the two processes overlap extensively (i.e., the cleft runs parallel to the basal lamina) the EO will approach unity. The estimated ratio (0.71) is indicative of a significant overlap. The sum of the projections amounts to 2.4% of the endothelial tube surface.

Elongated Mitochondria in Endfoot Processes

Mitochondria in endfeet are strikingly heterogenous with respect to size and shape. The 3D reconstructions (Fig. 6) revealed two main types of mitochondria: small/ovoid and elongated. Some of the elongated mitochondria were unbranched and could be traced retrogradely

into the astrocytic processes that connect the cell body with the endfeet. Others showed a very complex shape with several branches that appeared to extend into minor processes. The different mitochondria were intertwined to form large bundles that came into close apposition to the perivascular endfoot membrane.

DISCUSSION

The interest in astrocytic endfeet has recently been rekindled by the finding that these endfeet are involved in a number of transport processes at the brain–blood interface. Specifically, it has been proposed that water transport through the endfeet is rate-limiting in the development as well as resolution phase of brain edema (Amiry-Moghaddam and Ottersen, 2003; Papadopoulos and Verkman, 2007; Simard and Nedergaard, 2004). The validity of this hypothesis depends on the premise that the astrocytes form a continuous sheath around the brain microvessels.

Literature data are not consistent in regard to the degree of coverage offered by the perivascular glial sheath. Textbook drawings of endfeet (i.e., the cover page of Dermietzel et al., 2006) often indicate significant clefts that—if present—would shortcircuit any transport process mediated by the endfeet membranes or cancel the rate limitation imposed by diffusion through these. Importantly, it will be difficult to explain how endfeet could limit water transport if there are wide clefts between them that allow for free water diffusion.

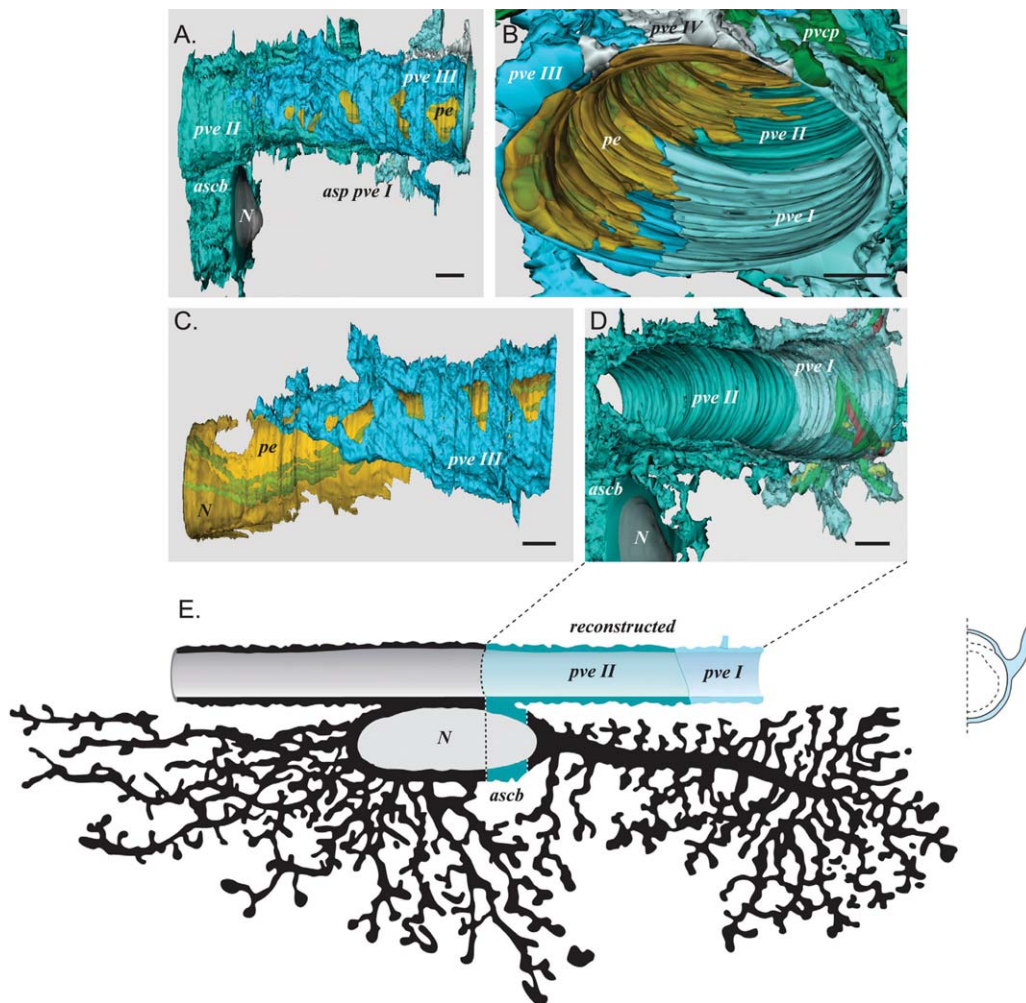


Fig. 2. The capillary surface is completely covered by a perivascular glial sheath. (A) This sheath surrounds the capillary and pericyte as presented in Fig. 1. A perivascular astrocyte with nucleus (*N*) and cell body (*ascb*) embraces (as *pve II*) the endothelial tube. The pericyte (*pe*) is seen through discontinuities in the endfoot indexed as *pve III*. Astrocytic processes (*asp*) from the endfeet stretch out in different directions. (B) Structure in A viewed from the right. All four endfeet (*pve I-IV*) in the reconstruction is represented together with the pericyte (*pe*). Part of a probable microglial cell process, indexed as a perivascular cell

process (*pvc*) and shown in Fig. 3, is seen peripheral to the glial sheath. (C,D) Removal of the pericyte, *pve III*, and *pve IV* (structures reconstructed in C) allows the remaining perivascular sheath (*pve I* and *II*) to be viewed from the inside (D). The most important feature in C is the six linearly arranged discontinuities of the third endfoot (*pve III*). (E) Elements reconstructed in D are shown in color and entered into a drawing adapted from Ramon y Cajal (1911). The cross-section (below right) corresponds to the one in Fig. 1(C) and shows *pve I* in blue. Scale bars = 1 μ m.

The aim of the present study was to provide a detailed 3D reconstruction of astrocytic endfeet based on EM analysis of serial ultrathin sections.

Previous Studies Addressing the Completeness of the Glial Sheath

Conclusions on the completeness of the perivascular astrocytic covering are found in a number of single section electron microscopic analysis. The covering is described as complete (Long et al., 1968; Luse, 1956; Mugnaini and Walberg, 1964; Mugnaini and Walberg, 1965a,b) or incomplete (Farquhar and Hartmann, 1957; Lange and Halata, 1972; Mori and Leblond, 1969). Maynard et al. (1957) reported 85% coverage in rat cerebral cortex while Wolff (1963) stated that endfeet covered 2/3 of the capillary

surface area in parietal cortex of rabbit. The discrepant statements regarding coverage are likely to reflect the fact that parts of the glial sheath are extremely thin. Thus, the present recordings show that the thickness of the sheath varies from 300 nm down to as thin as <20 nm. Obviously, endfeet as thin as these may easily escape detection in the absence of serial section analysis and 3D reconstruction.

In a confocal microscopic analysis, Kacem et al. (1998) concluded that the endfoot covering is incomplete. In this case the discontinuities likely reflect the choice of GFAP and S-100 β as marker molecule. In rodents, GFAP and S-100 β do not fill the endfeet, producing the false impression of endfoot discontinuity. In contrast, Oberheim et al. (2009) describe GFAP in human brain "to completely encompass the vessels, creating a cobblestone pattern along the vasculature". Simard et al. (2003) used the

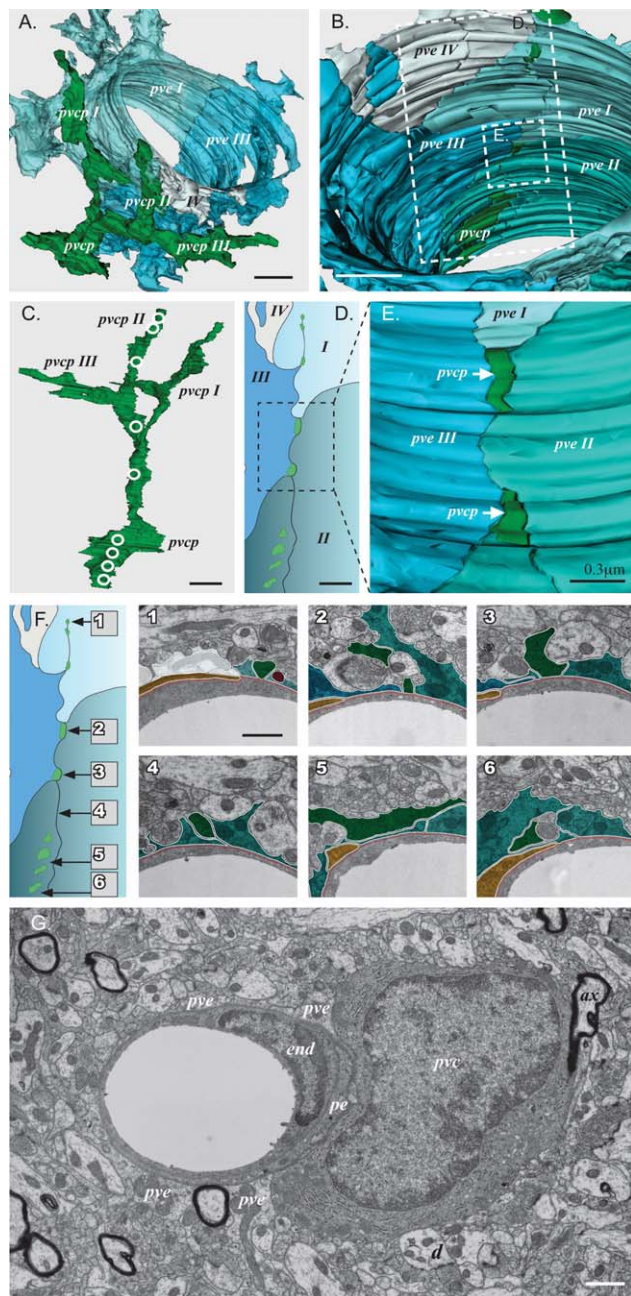


Fig. 3. Identification of a novel type of process that penetrates the perivascular glial sheath. (A) A perivascular cell process (*pvcp*), of probable microglial cell origin, climbs along the abluminal endfoot membranes and branches out in slender tendrils (*pvcp* I–III). Endfoot number two (*pve* II), from Fig. 2, is excluded from this model to gain overview. (B) Structure in A, rotated and tilted to view the perivascular processes from the inside. The perivascular cell process (*pvcp*) breaks through the glial sheath at several sites. Hatched areas are shown in D and E. (C) The perivascular cell process (*pvcp*) and its branches, shown from the same angle as in B but with the glial sheath removed. Sites of direct apposition to the basal lamina are encircled and correspond to the dark green areas in B, D–F. (D) Schematic drawing of elements in the larger of the two hatched areas in B. (E) The smaller of the hatched areas in B (also shown in D) is enlarged to provide a detailed view of two apposition sites (arrows). (F) Electron microscopic images of vessel wall at six different levels, indicated in diagram (left). Images 1–3 show direct attachment of the process to basal lamina, while there is an intervening endfoot in Images 4–6. (G) An endothelial tube (*end*), and the cell soma of a perivascular cell (*pvc*) in close proximity to perivascular endfeet (*pve*), a pericyte (*pe*), myelinated and nonmyelinated axons (*ax*) and dendrites (*d*). Scale bar = 1 μ m unless otherwise indicated.

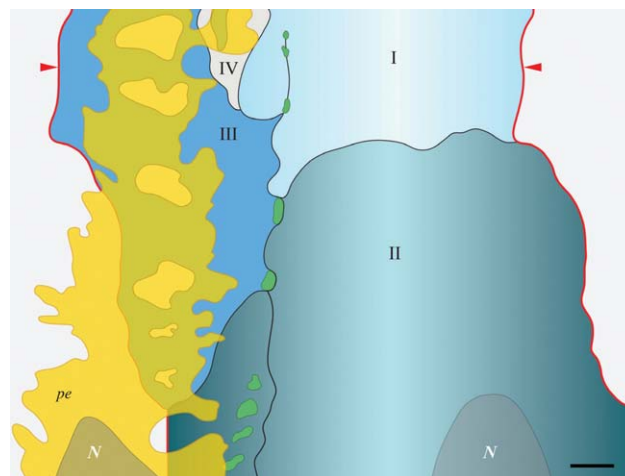


Fig. 4. The perivascular envelope shows high degree of complexity. This is an illustration of all the reconstructed perivascular structures as seen from the luminal side. Numbers I–IV represent four endfeet and the red line (arrowheads) indicates where the perivascular sheath was split to unfold. The third endfoot (*pve* III) which covers most of the pericyte has six discontinuities. The small green areas indicate the sites of penetration of the perivascular cell process (*pvcp*) described in Fig. 3. *N*, nucleus in astrocyte and pericyte. Scale bar = 1 μ m.

same technology (confocal microscopy) but nevertheless proposed that the endfoot coverage is complete based on AQP4 and GFAP immunolabeling. A study including the same markers to compare germinal matrix, cerebral cortex, and white matter in developing infants indicated incomplete covering (El-Khoury et al., 2006).

The previous analyses (except El-Khoury et al., 2006) did not include any morphometrical measurements or statistics. More thorough analysis of endfoot coverage were done by Sasaki and Mannen (1981) in the bullfrog (*Rana catesbeiana*) spinal cord and by Bär and Wolff (1977) in rat occipital cortex. The coverage was found to be 80–90% and 100%, respectively. Measurements in tissue from human parietal cerebral cortex (obtained at diagnostic biopsy or as perifocal tissue removed during tumor surgery) gave values ranging from 80 to 89% (Ambrosi et al., 1995; Bertossi et al., 1997; Virgintino et al., 1997).

Bertossi et al. (1989, 1993) and Roncali et al. (1989) introduced computer-based 3D reconstructions combined with morphometrical measurements to address the endfoot coverage. These were developmental studies in chick embryos. All three papers conclude with endfoot coverage of 12% at the 14th incubation day and 96% at the 20th i.d. So far, no 3D reconstructions addressing glial coverage have been performed in rats or in any other mammalian species. The reason for this is easy to comprehend: as succinctly stated by Hama et al. (1994), “the 3D shape of (glia) cell processes must be built up by reconstruction from many thin serial sections. This technique is only applicable for rather small areas because it requires tremendous time and effort.” These methodological limitations “have seriously hindered our understanding of glial structure” (Kosaka and Hama, 1986). Here we have attempted to advance our understanding of this important issue by taking advantage of recent advances in electron microscopy and software development.

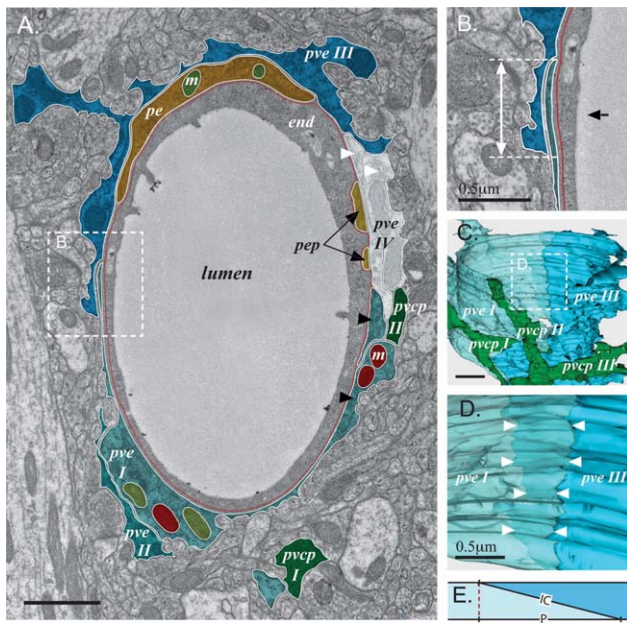


Fig. 5. Endfoot-endfoot overlap helps seal brain capillaries. (A) Electron microscopic image of capillary with four endfoot profiles (*pve I-IV*). The 3D reconstruction shows that each of the two pairs of profiles indicated by black or white arrowheads belongs to the same endfoot (black arrowheads: *pve I*; white arrowheads: *pve IV*). By reconstruction, the pericytic processes (*pep*) can be traced back to the pericyte (*pe*) in upper part of figure. All pericytic elements are embedded within the basal lamina and are thus easily identified in 2D images. Both endfeet and pericyte possess mitochondria (*m*). Two perivascular cell processes (*pvcp I and II*) are seen. The hatched area (enlarged in **B**) shows the endfoot-endfoot overlap. The double arrow in **B** represents the projection of the overlap, while the black arrow indicates the angle of view in **C**. (**C**) Endfoot *IV* is removed to view the remaining endfeet from the inside of the vessel (cf., Fig. 3A). In the hatched frame, enlarged in **D**, endfoot *I* (*pve I*) is made semitransparent to visualize the underlying endfoot *III* (*pve III*). The space between the two rows of arrowheads represents the extent of overlap. (**E**) Definition of the intercellular cleft length (*IC*) and the length of its projection (*P*). Scale bar = 1 μm unless otherwise indicated.

Functional Implications

Endfeet possess rate limiting role in water transport

Astrocytes are polarized in terms of structure as well as function (Wolff, 1970). There is now unequivocal evidence that the astrocytes are equipped with specialized membrane domains that serve specific transport functions. The abluminal endfeet membranes stand out as unique through their complement of high densities of aquaporin-4 (AQP4) molecules (Frigeri et al., 1995; Nielsen et al., 1997). These molecules are anchored by way of the dystrophin complex that is attached to the capillary basal lamina through a dystroglycan bridge (Amiry-Moghaddam and Ottersen, 2003; Neely et al., 2001).

Several studies have indicated that removal of perivascular AQP4 (through targeted disruption of α -syntrophin) significantly reduce the extent of brain edema after experimental stroke or hypotonic challenge (Amiry-Moghaddam et al., 2003, 2004; Vajda et al., 2002). Targeted disruption of the AQP4 gene similarly reduces the extent of brain edema (Manley et al., 2000). Removal of AQP4

from the perivascular membrane domain also interferes with the resolution of brain edema (Verkman et al., 2000). Based on these observations it has been concluded that the endfeet are rate limiting for water diffusion—if only under pathological conditions when water flux is high. Some doubt has been cast on these conclusions, as any discontinuity in the perivascular glial sheath would short-circuit any transport process. Here we provide evidence that the perivascular sheath indeed is continuous, lending credibility to the above conclusions on the rate limiting role of astrocytic endfeet.

A simple calculation based on our data illustrates our understanding of the glial sheath as a relative barrier to water flux. On average, we identified 2.5 transected intercellular clefts per vessel profile and the endfoot-endfoot clefts were measured to be ~ 20 nm wide. This gives a total cleft width of 50 nm per crosssectioned capillary, and a total cleft area of about $50,000 \text{ nm}^2$ per μm vessel. If the diameter of a capillary is $5 \mu\text{m}$, the circumference will be $\sim 15 \mu\text{m}$, and the area of $1 \mu\text{m}$ vessel $15 \mu\text{m}^2$ (15 million nm^2). Consequently, the mouths of the clefts add up to a total of 0.3% of the area of the endothelial tube. In contrast, 20% of crosssectioned neuropil represent intercellular space (Lehre and Danbolt, 1998). This implies that the total area available for water flux is much larger in neuropil than across the the perivascular glial sheath.

The continuous coverage provided by the endfeet and the considerable overlap of adjacent endfoot processes therefore imply that perivascular glial coverage can control the exchange of water and metabolites between blood and brain in situations of high flux rates. Obviously, the glial coverage does not constitute a barrier on a par with the endothelial cell layer as the adjacent glial processes are coupled by gap junctions rather than tight junctions (Simard et al., 2003). However, the narrow openings and small number of intercellular clefts in contact with the endothelial tube afford a relative diffusion barrier that may be functionally significant in pathological situations (Brightman, 2002). Data presented in this study will allow calculations of the extent to which diffusion is restricted by the perivascular astrocyte processes and the clefts between them.

Glial sheath and intercellular Ca^{2+} signaling

Another implication of our finding of a complete and overlapping endfoot coverage is that the endfeet may provide a continuous avenue for signaling along the brain microvessels (Iadecola and Nedergaard, 2007; Nedergaard et al., 2003; Scemes and Giaume, 2006). At sites of overlap the endfeet express gap junctions (composed mainly of Cx43) that ensure direct coupling and Ca^{2+} transfer (Simard et al., 2003). As a result calcium waves are allowed to propagate along the vessel wall. Following electrical stimulation these waves are shown to migrate several tens of micrometer along cerebral microvessels (Simard et al., 2003). Importantly, calcium transients in astrocyte endfeet may be involved in the regulation of

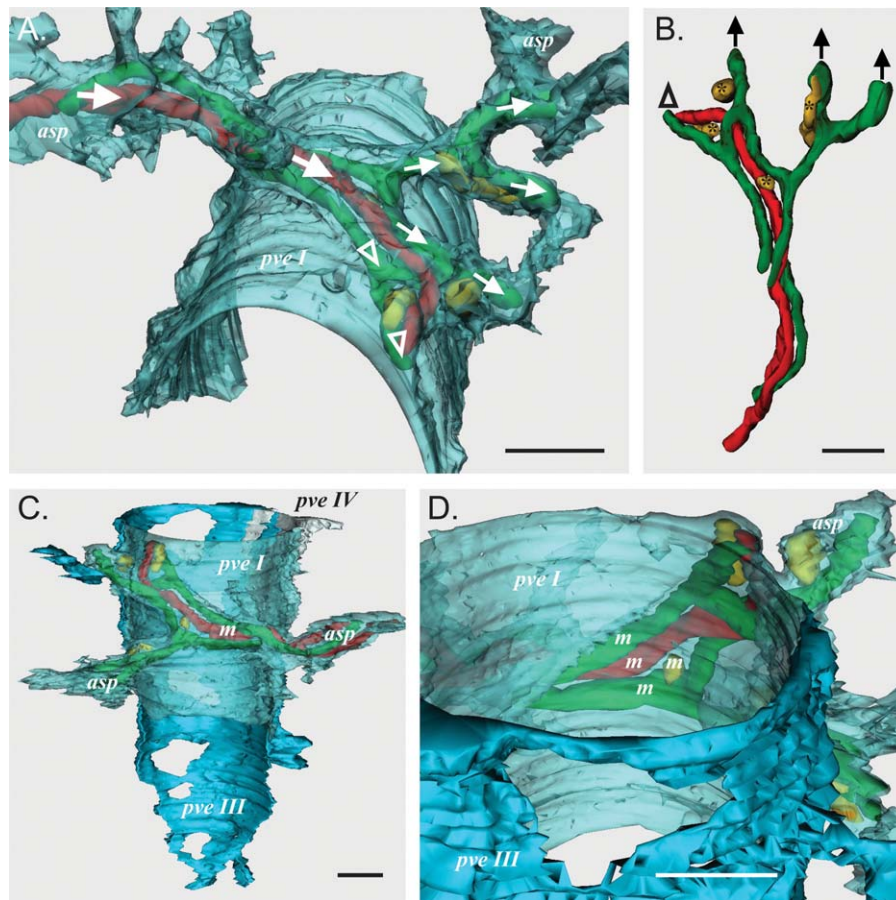


Fig. 6. Endfoot processes contain elongated mitochondria. (A) A semitransparent 3D reconstruction of a perivascular endfoot (*pve I*) seen from an abluminal perspective. The footplate is complete and covers about half the circumference of the vessel wall. Elongated mitochondria (arrows) enter the endfoot tangentially through the left process (*asp*) and leave through four processes on the right hand side. Open arrowheads indicate the fourth endfoot process with mitochondria. The lower of the open arrowheads in A corresponds to the open arrowhead in B.

(B) Representation of the mitochondria (from *pve I*) without any endfeet and processes. Two main types of mitochondrion occur: long (labelled in A) and small (asterisks). (C) Endfoot number one (*pve I*) together with number three (*pve III*) and four (*pve IV*). (D) Model C turned around 180 degrees and tilted towards the reader, allows a glimpse into the endfoot tract through the adluminal membrane. Most prominent are the passing mitochondria (*m*), and the hole in endfoot number three (*pve III*) covering the pericyte in Fig. 2C. Scale bars = 1 μ m.

blood flow (Mulligan and MacVicar, 2004; Scemes et al., 1998; Takano et al., 2006; Zonta et al., 2003).

Calcium waves do not only propagate between endfeet, but also through neighboring astrocytes organized in functional domains within the pan-glia syncytium (Bushong et al., 2002; Ogata and Kosaka, 2002). In its role as a paracrine messenger acting on purinergic receptors, ATP has been shown to complement the more direct signaling pathway through gap junctions (Arcuino et al., 2002). Our data show numerous elongated mitochondria in astrocytic somata and in their radiating processes. The ATP produced from these mitochondria may double as signaling molecules and energy quanta.

Direct contacts between pericytes and neuropil through discontinuities in the endfoot

The most established functional property of pericytes is their ability to contract (Rucker et al., 2000). One important question is how they are activated. Our

reconstruction shows longitudinally oriented discontinuities in the glial sheath on the abluminal surface of the pericytes. These discontinuities open for direct contact between pericytes and neuropil elements and could provide avenues for the chemical signals that evoke pericyte-mediated capillary constriction (Peppiatt et al., 2006). This hypothesis of functional coupling between brain parenchyma and the vessel wall would be strengthened if there are any specific profiles that could be interpreted as terminals abutting on the abluminal face of the pericytes.

Actually, studies based on serial sections (Paspalas and Papadopoulos, 1996) have shown perivascular nerve terminals to interrupt the astrocytic ensheathment resulting in direct contact with the basal lamina of capillaries. Other single section analyses have revealed higher frequency of terminals in the immediate vicinity (0.25 μ m or less) of the microvessels compared with larger distances (Cohen et al., 1997), and that pericapillary axon terminals constitute a morphologically distinct population compared with more distant terminals

(Lukaszyk et al., 1996). However, we did not recognize any specific peri-pericytic organization of neuropil in our material, and for this reason studies are in progress to reconstruct the neuropil elements facing the above discontinuities.

Juxtavascular microglia

Only in a few sites were the perivascular sheath found to be discontinuous over the endothelial basal lamina. These discontinuities were filled by processes that emanated from cells with an electron dense cytoplasmic matrix. These cells were classified as juxtavascular microglia (Grossmann et al., 2002; Lassmann et al., 1991). Their identity as such is tentative, as these cells did not show inclusion bodies (Peters et al., 1991). Microglia are closely related to the monocyte/macrophage lineage and those related to blood-brain barrier are divided into perivascular cells (enclosed within the basal lamina) and juxtavascular microglia (directly apposed to the basal lamina; Gehrmann et al., 1995). The latter is a true intraparenchymal cell and has been observed to be recruited from neuropil to the surface of capillaries after injury. Some of these cells have the capacity to move up to 40 $\mu\text{m}/\text{h}$ along the vessel wall and are believed to interact with components of the blood-brain barrier or to present antigens to circulating immune cells (Grossmann et al., 2002). This is the first 3D study to demonstrate that putative microglial processes establish direct contact with the basal lamina of brain microvessels.

CONCLUSION

This study, from hippocampal stratum moleculare CA1, should lay to rest the longstanding debate as to whether the endfeet form a continuous or discontinuous covering of the microvessels in brain. The 3D reconstruction data indicate that the covering is close to complete and that the very few discontinuities that exist are filled by processes extending from juxtavascular cells. Other studies have demonstrated perivascular nerve terminals that interrupt the astrocytic ensheathment (Edvinsson and Hamel, 2002). Taken together with previous studies our data support the idea that, under pathophysiological conditions, the perivascular endfoot covering can add to the barrier function of the endothelia and restrict transport or diffusion across the blood-brain interface. A limitation of our study is that it is restricted to one particular brain structure—albeit one of the most intensively studied of all—and that we cannot generalize across brain regions and species. This limitation reflects the very nature of 3D reconstructions.

ACKNOWLEDGMENTS

The authors thank Gunnar Lothe, Carina Knudsen, Espen Petersheim, and Bashir Hakim for excellent

technical assistance, Paworn Nuntagij for initial introduction to the 3D-software, Kristen Harris and the Reconstruct Users Group for technical advice.

REFERENCES

- Ambrosi G, Virgintino D, Benaglio V, Maiorano E, Bertossi M, Roncali L. 1995. Glial cells and blood-brain barrier in the human cerebral cortex. *Ital J Anat Embryol* 100 (Suppl 1):177–184.
- Amiry-Moghaddam M, Otsuka T, Hurn PD, Traystman RJ, Haug FM, Froehner SC, Adams ME, Neely JD, Agre P, Ottersen OP, Bhardwaj A. 2003. An alpha-syntrophin-dependent pool of AQP4 in astroglial end-feet confers bidirectional water flow between blood and brain. *Proc Natl Acad Sci USA* 100:2106–2111.
- Amiry-Moghaddam M, Ottersen OP. 2003. The molecular basis of water transport in the brain. *Nat Rev Neurosci* 4:991–1001.
- Amiry-Moghaddam M, Xue R, Haug FM, Neely JD, Bhardwaj A, Agre P, Adams ME, Froehner SC, Mori S, Ottersen OP. 2004. Alpha-syntrophin deletion removes the perivascular but not endothelial pool of aquaporin-4 at the blood-brain barrier and delays the development of brain edema in an experimental model of acute hyponatremia. *FASEB J* 18:542–544.
- Arcuino G, Lin JH, Takano T, Liu C, Jiang L, Gao Q, Kang J, Nedergaard M. 2002. Intercellular calcium signaling mediated by point-source burst release of ATP. *Proc Natl Acad Sci USA* 99:9840–9845.
- Ballabh P, Braun A, Nedergaard M. 2004. The blood-brain barrier: An overview: Structure, regulation, and clinical implications. *Neurobiol Dis* 16:1–13.
- Bär T, Wolff JR. 1977. Morphometry of interendothelial and glio-vascular contacts of rat brain capillaries during postnatal development. *Bibl Anat* 15:514–517.
- Bertossi M, Ribatti D, Nico B, Virgintino D, Mancini L, Roncali L. 1989. Computerized three-dimensional reconstruction of the developing blood-brain barrier. *Acta Neuropathol* 79:48–51.
- Bertossi M, Roncali L, Nico B, Ribatti D, Mancini L, Virgintino D, Fabiani G, Guidazzoli A. 1993. Perivascular astrocytes and endothelium in the development of the blood-brain barrier in the optic tectum of the chick embryo. *Anat Embryol (Berl)* 188:21–29.
- Bertossi M, Virgintino D, Maiorano E, Occhiogrosso M, Roncali L. 1997. Ultrastructural and morphometric investigation of human brain capillaries in normal and peritumoral tissues. *Ultrastruct Pathol* 21:41–49.
- Brightman MW. 2002. The brain's interstitial clefts and their glial walls. *J Neurocytol* 31:595–603.
- Bushong EA, Martone ME, Jones YZ, Ellisman MH. 2002. Protoplasmic astrocytes in CA1 stratum radiatum occupy separate anatomical domains. *J Neurosci* 22:183–192.
- Casella JP, Hay J, Lawson SJ. 1997. The rat nervous system. An introduction to preparatory techniques. England: Wiley.
- Cohen Z, Molinatti G, Hamel E. 1997. Astroglial and vascular interactions of noradrenaline terminals in the rat cerebral cortex. *J Cereb Blood Flow Metab* 17:894–904.
- Danbolt NC, Lehre KP, Dehnes Y, Chaudry FA, Levy LM. 1998. Localization of transporters using transporter-specific antibodies. *Methods Enzymol* 296:388–407.
- Dermietzel R, Spray DC, Nedergaard M, editors. 2006. Blood-brain barriers: From ontogeny to artificial interfaces. Weinheim, Germany: Wiley-VCH Verlag.
- Díaz-Flores L, Gutiérrez R, Varela H, Rancel N, Valladares F. 1991. Microvascular pericytes: A review of their morphological and functional characteristics. *Histol Histopathol* 6:269–286.
- Duvernoy HM. 2005. The human hippocampus. Functional anatomy, vascularization and serial sections with MRI, 3rd ed. Berlin: Springer-Verlag.
- Edvinsson L, Hamel E. 2002. Perivascular nerves in brain vessels. In: Edvinsson L, Krause DN, editors. Cerebral blood flow and metabolism, 2nd ed. Philadelphia, PA: Lippincott Williams and Wilkins. pp 43–67.
- El-Khoury N, Braun A, Hu F, Pandey M, Nedergaard M, Lagamma EF, Ballabh P. 2006. Astrocyte end-feet in germinal matrix, cerebral cortex, and white matter in developing infants. *Pediatr Res* 59:673–679.
- Farquhar MG, Hartmann JF. 1957. Neuroglial structure and relationships as revealed by electron microscopy. *J Neuropathol Exp Neurol* 16:18–39.
- Fiala JC. 2005. Reconstruct: a free editor for serial section microscopy. *J Microsc* 224:211.
- Frigeri A, Gropper MA, Umenishi F, Kawashima M, Brown D, Verkman AS. 1995. Localization of MIWC and GLIP water channel homologs in neuromuscular, epithelial and glandular tissues. *J Cell Sci* 108: 2993–3002.

- Gehrmann J, Matsumoto Y, Kreutzberg GW. 1995. Microglia: Intrinsic immuneffector cell of the brain. *Brain Res Brain Res Rev* 20:269–287.
- Glees P. 1955. *Neuroglia. Morphology and function.* Oxford: Blackwell.
- Golgi C. 1871. *Contribuzione alla fina Anatomia degli organi centrali del sistema nervoso.* Bologna: Rivista clinica di Bologna.
- Gotow T, Hashimoto PH. 1984. Plasma membrane organization of astrocytes in elasmobranchs with special reference to the brain barrier system. *J Neurocytol* 13:727–742.
- Grossmann R, Stence N, Carr J, Fuller L, Waite M, Dailey ME. 2002. Juxtavascular microglia migrate along brain microvessels following activation during early postnatal development. *Glia* 37:229–240.
- Hama K, Arai T, Kosaka T. 1994. Three-dimensional organization of neuronal and glial processes: High voltage electron microscopy. *Microsc Res Tech* 29:357–367.
- Harris KM, Perry E, Bourne J, Feinberg M, Ostroff L, Hurlburt J. 2006. Uniform serial sectioning for transmission electron microscopy. *J Neurosci* 26:12101–12103.
- Iadecola C, Nedergaard M. 2007. Glial regulation of the cerebral microvasculature. *Nat Neurosci* 10:1369–1376.
- Kacem K, Lacombe P, Seylaz J, Bonvento G. 1998. Structural organization of the perivascular astrocyte endfeet and their relationship with the endothelial glucose transporter: A confocal microscopy study. *Glia* 23:1–10.
- Kosaka T, Hama K. 1986. Three-dimensional structure of astrocytes in the rat dentate gyrus. *J Comp Neurol* 249:242–260.
- Landis DMD, Reese TS. 1974. Arrays of particles in freeze-fractured astrocytic membranes. *J Cell Biol* 60:316–320.
- Lange W, Halata Z. 1972. Ultrastructure of capillaries in the cerebellar cortex and the pericapillary compartment. *Z Zellforsch Mikrosk Anat* 128:83–99.
- Lassmann H, Zimprich F, Vass K, Hickey WF. 1991. Microglial cells are a component of the perivascular glia limitans. *J Neurosci Res* 28:236–243.
- Lehre KP, Danbolt NC. 1998. The number of glutamate transporter subtype molecules at glutamatergic synapses: Chemical and stereological quantification in young adult rat brain. *J Neurosci* 18:8751–8757.
- Lehre KP, Levy LM, Ottersen OP, Storm-Mathisen J, Danbolt NC. 1995. Differential expression of two glial glutamate transporters in the rat brain: Quantitative and immunocytochemical observations. *J Neurosci* 15:1835–1853.
- Long DM, Bodenheimer TS, Hartmann JF, Klatzo I. 1968. Ultrastructural features of the shark brain. *Am J Anat* 122:209–236.
- Lukaszuk I, Kraszpulski M, Wrzółkowska T. 1996. Pericapillary and distant axon terminals in the nuclei of the cat amygdala: A morphometric study. *Anat Embryol* 193:297–302.
- Luse SA. 1956. Electron microscopic observations of the central nervous system. *J Biophys Biochem Cytol* 2:531–542.
- Manley GT, Fujimura M, Ma T, Noshita N, Filiz F, Bollen AW, Chan P, Verkman AS. 2000. Aquaporin-4 deletion in mice reduces brain edema after acute water intoxication and ischemic stroke. *Nat Med* 6:159–163.
- Maynard EA, Schultz RL, Pease DC. 1957. Electron microscopy of the vascular bed of rat cerebral cortex. *Am J Anat* 100:409–433.
- Mercier F, Mambie S, Hatton GI. 2006. Brain Macrophages: Enigmas and conundrums. In: Dermietzel R, Spray DC, Nedergaard M, editors. *Blood-brain barriers: From ontogeny to artificial interfaces.* Weinheim, Germany: Wiley-VCH Verlag. pp 129–165.
- Mori S, Leblond CP. 1969. Electron microscopic features and proliferation of astrocytes in the corpus callosum of the rat. *J Comp Neurol* 137:197–225.
- Mugnaini E, Walberg F. 1964. Ultrastructure of neuroglia. *Ergeb Anat Entwicklungsgesch* 37:194–236.
- Mugnaini E, Walberg F. 1965a. The perivascular elements in the central nervous system. An electron microscopical study. *Acta Neurol Scand Suppl* 13:629–636.
- Mugnaini E, Walberg F. 1965b. The fine structure of the capillaries and their surroundings in the cerebral hemispheres of *Myxine Glutinosa*. *Z Zellforsch Mikrosk Anat* 66:333–351.
- Mulligan SJ, MacVicar BA. 2004. Calcium transients in astrocyte endfeet cause cerebrovascular constrictions. *Nature* 431:195–199.
- Nedergaard M, Ransom B, Goldman SA. 2003. New roles for astrocytes: Redefining the functional architecture of the brain. *Trends Neurosci* 26:523–530.
- Neely JD, Amiry-Moghaddam M, Ottersen OP, Froehner SC, Agre P, Adams ME. 2001. Syntrophin-dependent expression and localization of Aquaporin-4 water channel protein. *Proc Natl Acad Sci USA* 98:14108–14113.
- Neuhaus J. 1990. Orthogonal arrays of particles in astroglial cells: Quantitative analysis of their density, size, and correlation with intramembranous particles. *Glia* 3:241–251.
- Nielsen S, Nagelhus EA, Amiry-Moghaddam M, Bourque C, Agre P, Ottersen OP. 1997. Specialized membrane domains for water transport in glial cells: High-resolution immunogold cytochemistry of aquaporin-4 in rat brain. *J Neurosci* 17:171–180.
- Oberheim NA, Takano T, Han X, He W, Lin JH, Wang F, Xu Q, Wyatt JD, Pilcher W, Ojemann JG, Ransom BR, Goldman SA, Nedergaard M. 2009. Uniquely hominid features of adult human astrocytes. *J Neurosci* 29:3276–3287.
- Ogata K, Kosaka T. 2002. Structural and quantitative analysis of astrocytes in the mouse hippocampus. *Neuroscience* 113:221–233.
- Papadopoulos MC, Verkman AS. 2007. Aquaporin-4 and brain edema. *Pediatr Nephrol* 22:778–784.
- Paspalas CD, Papadopoulos GC. 1996. Ultrastructural relationships between noradrenergic nerve fibers and non-neuronal elements in the rat cerebral cortex. *Glia* 17:133–146.
- Peppiatt CM, Howarth C, Mobbs P, Attwell D. 2006. Bidirectional control of CNS capillary diameter by pericytes. *Nature* 443:700–704.
- Peters A, Palay SL, Webster H. 1991. *The fine structure of the nervous system. Neurons and their supporting cells*, 3rd ed. Oxford University Press. Chapter 7, pp 273–311.
- Rash JE, Davidson KG, Yasumura T, Furman CS. 2004. Freeze-fracture and immunogold analysis of aquaporin-4 (AQP4) square arrays, with models of AQP4 lattice assembly. *Neuroscience* 129:915–934.
- Ramón y Cajal S. 1911. *Histologie du Système Nerveux de l'Homme et des Vertébrés.* Paris. Translated by Swanson N, Swanson LW. 1995. *Histology of the nervous system of man and vertebrates.* Oxford University Press. p 196.
- Roncali L, Bertossi M, Ribatti D, Nico B, Virgintino D, Mancini L. 1989. Perivascular glia-endothelium relationships in the developing cerebral vessels. A three-dimensional computer aided study. *Prog Clin Biol Res* 295:383–387.
- Rucker HK, Wynder HJ, Thomas WE. 2000. Cellular mechanisms of CNS pericytes. *Brain Res Bull* 51:363–369.
- Sasaki H, Mannen H. 1981. Morphological analysis of astrocytes in the bullfrog (*Rana catesbeiana*) spinal cord with special reference to the site of attachment of their processes. *J Comp Neurol* 198:13–35.
- Scemes E, Dermietzel R, Spray DC. 1998. Calcium waves between astrocytes from Cx43 knockout mice. *Glia* 24:65–73.
- Scemes E, Giaume C. 2006. Astrocyte calcium waves: What they are and what they do. *Glia* 54:716–725.
- Simard M, Arcuino G, Takano T, Liu QS, Nedergaard M. 2003. Signaling at the gliovascular interface. *J Neurosci* 23:9254–9262.
- Simard M, Nedergaard M. 2004. The neurobiology of glia in the context of water and ion homeostasis. *Neuroscience* 129:877–896.
- Takano T, Tian GF, Peng W, Lou N, Libionka W, Han X, Nedergaard M. 2006. Astrocyte-mediated control of cerebral blood flow. *Nat Neurosci* 9:260–267.
- Vajda Z, Pedersen M, Füchtbauer EM, Wertz K, Stødkilde-Jørgensen H, Sulyok E, Dóczi T, Neely JD, Agre P, Frøkiær J, Nielsen S. 2002. Delayed onset of brain edema and mislocalization of aquaporin-4 in dystrophin-null transgenic mice. *Proc Natl Acad Sci USA* 99:13131–13136.
- Verkman AS, Yang B, Song Y, Manley GT, Ma T. 2000. Role of water channels in fluid transport studied by phenotype analysis of aquaporin knockout mice. *Exp Physiol* 85:233S–241S.
- Virchow R. 1858. *Die Cellularpathologie in ihrer Begründung auf physiologische und pathologische Gewebelehre.* Berlin: Verlag von August Hirschwald.
- Virgintino D, Monaghan P, Robertson D, Errede M, Bertossi M, Ambrosi G, Roncali L. 1997. An immunohistochemical and morphometric study on astrocytes and microvasculature in the human cerebral cortex. *Histochem J* 29:655–660.
- Wolburg H. 1995. Orthogonal arrays of intramembranous particles: A review with special reference to astrocytes. *J Hirnforsch* 36:239–258.
- Wolff J. 1963. Contributions to the ultrastructure of the capillaries in the normal cerebral cortex. *Z Zellforsch Mikrosk Anat* 60:409–431.
- Wolff JR. 1970. The astrocyte as link between capillary and nerve cell. *Triangle* 9:153–164.
- Zonta M, Angulo MC, Gobbo S, Rosengarten B, Hossmann KA, Pozzan T, Carmignoto G. 2003. Neuron-to-astrocyte signaling is central to the dynamic control of brain microcirculation. *Nat Neurosci* 6:43–50.